Catalysis Science & Technology

ROYAL SOCIETY OF CHEMISTRY

PAPER

View Article Online
View Journal | View Issue

Cite this: *Catal. Sci. Technol.*, 2023, **13**, 1696

Supported boron-based catalysts for oxidative dehydrogenation of light alkanes to olefins

Wen-Duo Lu, Bin Qiu, Zhan-Kai Liu, Fan Wu and An-Hui Lu *

Received 10th December 2022,
Accepted 9th February 2023

DOI: 10.1039/d2cy02098j

rsc.li/catalysis

Boron-based catalysts have shown great fundamental and practical value in oxidative dehydrogenation (ODH) of light alkanes to olefins. Particularly, supported boron-based catalysts exhibit superior specific activity with highly dispersed active sites and adjustable structures, which can be used to understand the reaction pathway and promotion effect of the microenvironment in a clear manner. This review surveyed the structural characteristics of several important supported boron-based catalysts and their catalytic performance in ODH of light alkanes. The similarities and differences in the origin of active sites and kinetic behaviors over these supported catalysts were summarized and discussed. The interaction between the active boron species and support still plays a crucial role in the stability and activity of the catalysts. Moreover, the potential research directions for the application of highly active and stable boron-based catalysts in ODH of light alkanes to olefins were prospected.

1. Introduction

Light olefins, the most important feedstocks in the petrochemical industry for the production of fine chemicals, are traditionally produced by petroleum-derived steam cracking and fluid catalytic cracking (FCC).[1–3] Nevertheless, the petroleum-derived processes are still far from meeting the forecast market demand for olefins.[4,5] Recently, the discovery of shale gas which contains abundant light alkanes has given a friendly boost in obtaining olefins from the gas-based dehydrogenation process.[1,6,7] The on-purpose technology of catalytic dehydrogenation of alkanes represents an economical and environmentally friendly route that can be used by industry for the production of particular olefins.[8] The advantages of high purity and energy efficiency make it more profitable in the current market conditions. Several processes for the direct dehydrogenation of light alkanes have emerged as industrial technologies to produce light olefins. Owing to the endothermic reaction nature of the direct dehydrogenation process, a high temperature is required to achieve a reasonable conversion and high yield of target olefins, which restricts the reaction efficiency. Moreover, sintering and coking are promoted dramatically under tough operating conditions, leading to accelerated catalyst deactivation, thus requiring regeneration of the catalysts frequently under harsh conditions.[9,10]

State Key Laboratory of Fine Chemicals, Liaoning Key Laboratory for Catalytic Conversion of Carbon Resources, School of Chemical Engineering, Dalian University of Technology, Dalian 116024, P. R. China.
E-mail: anhuilu@dlut.edu.cn

Oxidative dehydrogenation (ODH) of alkanes to olefins, characterized by exothermic thermodynamics, non-equilibrium limit and coke resistance, is a burgeoning alternative to direct dehydrogenation.[11–18] These reaction characteristics allow it to proceed at lower temperatures and without catalyst regeneration protocols. Previously, the research interest has been concentrated on transition metal oxides or alkaline-earth metal oxychlorides in the ODH reaction of light alkanes.[4,14,19] Indeed, the selectivity control of olefins is still a great challenge in ODH reaction systems, since the formed electron-rich allylic carbon atoms in olefins react more easily with oxygen over the metal oxide catalysts, resulting in the formation of over-oxidation products and the reduction of the selectivity to desired olefins. Therefore, there is an urgent need to develop innovative catalyst systems that can produce highly selective olefins under oxidative conditions.

The discovery of functionalized hexagonal boron nitride featuring high activity and selectivity to olefins with less formation of CO_2 lights up the dawn in this field.[20–24] Since then, the new catalytic system has drawn extensive research interest in the fields of materials and catalysis science. A series of boron-based catalysts was synthesized and has similar novel activity with boron nitride, which opens up a new sight in C–H bond selective cleavage.[25–27] The research on the boron-based catalyst is mainly focused on bulk materials such as BN, B_4C, SiB_6, and so on. Besides, higher activity is usually obtained by adjusting the catalytic process for these bulk catalysts.[28] For these boron-containing materials, XPS, ssNMR and infrared spectroscopy characterizations demonstrated that the formed B–O/B–OH on the surface of the materials following the catalytic ODH of alkanes could be the active species. Although

we observed the B–O species during the ODH reaction, these observations do not allow us to irrefutably conclude the clear structure of active boron sites. The synthesis of catalysts with structurally controlled B–O species could contribute to enhancing the identification of active sites for boron-based catalysts and potentially understand the mechanism of the ODH reaction easily.

Considering the diversity of heterogeneous catalysts, supported catalysts have drawn much attention in materials and chemistry science, due to their advantageous features, for instance, high efficiency, simple preparation, adjustable structure, and highly dispersed active sites for catalytic reactions.[29,30] It is easier to control the structure of the active site and understand the mechanism when using supported boron-based catalysts. In addition, considering that boron oxide with a low melting point and low viscosity is almost always found in vitreous form,[31] dispersal and stabilization of this active species by suitable supports will further enhance the catalytic activity. In this review, we will summarize the recent progress of the rational design of novel supported boron-based catalytic materials, identifying active sites, and essential insights into the catalytic mechanism. The interaction between boron species and supports, and how the supports affect the reaction will be discussed to inspire the innovation of supported boron-based catalysts for ODH reactions. In the end, according to the reaction characteristics of supported boron-based catalysts, future perspectives toward the production of highly active supported catalysts are proposed.

2. Metal oxide support

The study of boron-based materials supported on metal oxides to catalyze the oxidation of alkanes could be traced back to the 1980s. Given the strong dehydrogenation capacity of basic oxides and oxygen addition capacity of acid oxides, Otsuka *et al.*[32] used a MgO and B_2O_3 mixture for partial oxidation of methane to formaldehyde. The higher yield of formaldehyde was observed compared with only the B_2O_3 catalyst, indicating the synergistic effect in this acid–base bifunctional catalyst.

Later, boron oxide catalysts supported on various metal oxides (Al_2O_3, La_2O_3, MgO, TiO_2, CaO, ZnO) were prepared for the partial oxidation of ethane to ethylene and acetaldehyde, where most catalysts were more selective for acetaldehyde formation than B_2O_3 without supports.[33] Particularly, B_2O_3(30)–Al_2O_3 showed the best performance with a yield of ethylene of 14.6% and acetaldehyde of 1.03% when the ethane conversion was 38% at 550 °C. The crystalline B_2O_3 was regarded as the active site for ethylene formation, while acetaldehyde was formed not *via* ethylene but directly from ethane on other active sites. When B_2O_3 was supported on Al_2O_3, the selectivity to CO increased to 31%, indicating that the deep-oxidation routes were enhanced by adding Al_2O_3. Due to the unique activity of B_2O_3–Al_2O_3 catalysts, Otsuka *et al.*[34] further studied the active sites and reaction mechanism by a series of characterizations and kinetic experiments. XPS spectra showed two peaks at 192.2 eV and 189.7 eV assigned to crystalline B_2O_3 and cluster-type B_2O_3, respectively. According to the variation trend in product yield and boron oxide amount with increasing loading content, the active site for ethylene formation was ascribed to the crystalline B_2O_3, which was responsible for the activation of the initial C–H bond in ethane, while the cluster-type B_2O_3 was active for the formation of acetaldehyde. The formation rate exhibited a second order dependence on the pressure of ethane (Fig. 1a). Hence, the chain reaction mechanism was proposed, which was different from the mechanism of Mars–van Krevelen followed by metal oxide catalysts. Meanwhile, the highly dispersed boron oxide could poison the active site on alumina for deep-oxidation, and suppress the formation of CO and CO_2. To create a layer of boron oxide with higher dispersion on the surface, Auroux *et al.*[35] used chemical vapour deposition (CVD) to prepare alumina–boria catalysts. The 30 wt% boron oxide loaded on non-porous Al_2O_3 showed a maximum of ethane conversion (18.7%) with 16.7% yield of ethylene. Boron oxide was proposed to be the critical species to form ethyl hydroperoxides and to suppress total oxidation, leading to the high selectivity to ethylene. Given the strong capacity of yttria stabilized zirconia (YSZ) for oxygen ion transport, Otsuka *et al.*[36] prepared a YSZ supported B_2O_3 catalyst for the ODH reaction of ethane. The electrocatalytic cell experiments and XPS indicated that the generation of peroxide, which was responsible for the activation of ethane, was promoted through the transfer of oxygen from the bulk of YSZ to B_2O_3.

Boron oxide catalysts promoted by metal oxides were also investigated in the propane selective oxidation reaction.[37] Through H–D and oxygen isotopic exchange reactions, Buyevskaya *et al.*[38] reported that the dissociative adsorption of propane and oxygen was suppressed by the additional boron to eliminate the hydroxyl groups on Al_2O_3 in B_2O_3–Al_2O_3 catalysts. These hydroxyl groups would lead to non-selective products, decreasing the selectivity to propylene. Based on the comparison between three types of catalysts (V_2O_5-based catalyst, rare-earth oxide-based catalyst, and B_2O_3–Al_2O_3 catalyst), the higher selectivity to propylene on B_2O_3–Al_2O_3 was attributed to the gas reactions of propyl radicals after their desorption from the surface.[39] Later, Buyevskaya *et al.*[40] investigated boron oxide catalysts supported on various metal oxides (Al_2O_3, TiO_2, ZrO_2, and MgO) for the propane partial oxidation reaction. The B_2O_3/Al_2O_3 catalyst exhibited the best activity with 45–48% propane conversion and 22% propylene yield. The ^{11}B MAS NMR spectra and XRD demonstrated that the trigonal BO_3 species in both amorphous and crystalline phases was active for propylene formation (Fig. 1b and c). These species would leach through interaction with water formed in the reaction environment, leading to the deactivation of the catalyst. In addition, the $Al_6B_8O_{21}$ phase generated by the interaction between boron and aluminum was relative to the production of oxygenates.

In conclusion, adopting metal oxides as supports of boron oxide catalysts could uniformly disperse the active sites and

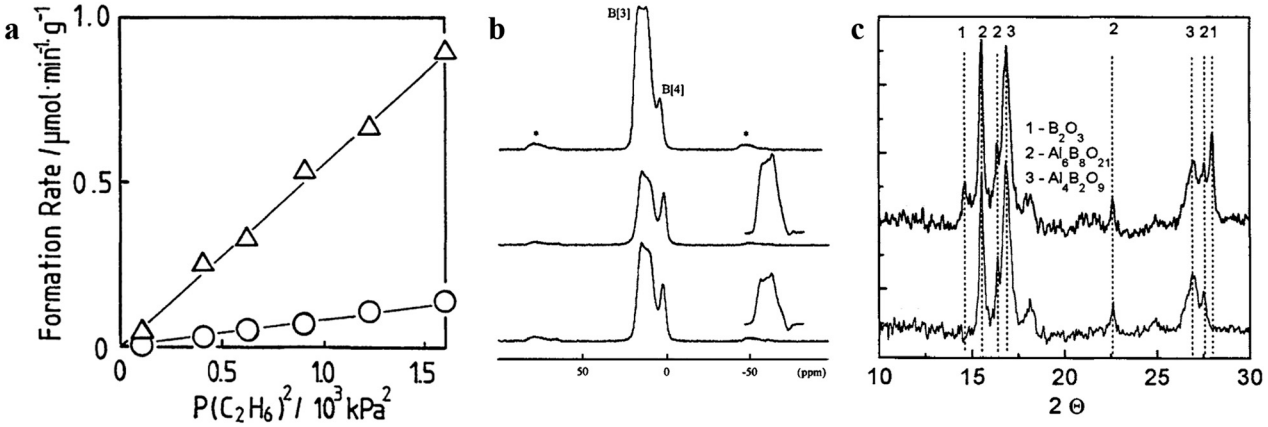

Fig. 1 (a) Effect of the pressure of ethane on partial oxidation of ethane over $B_2O_3(30)$–Al_2O_3. Ethylene (△) and acetaldehyde (○). Reaction temperature = 773 K, weight of catalyst = 0.05 g, flow rate = 100 mL min^{-1}, $P(O_2)$ = 10 kPa;[34] (b) ^{11}B MAS NMR spectra of B_2O_3/Al_2O_3 catalyst;[40] (c) X-ray diagrams of B_2O_3/Al_2O_3 catalyst.[40] Reproduced from ref. 34 with permission from the Chemical Society of Japan, copyright 1990. Reproduced from ref. 40 with permission from Elsevier Ltd, copyright 1998.

regulate the electronegativity of boron species, promoting the conversion of alkanes. However, for ODH of light alkanes to olefins in previous studies, the acid sites or formation of non-stoichiometric oxygen on the metal oxide surface could catalyze unwanted deep-oxidation reactions to generate a large amount of CO_2.[41] Moreover, the deactivation of these boron oxide catalysts supported on metal oxides through the loss of active boron species was also a serious problem that restricted the development of industrialization. Therefore, it was important to develop supported boron-based catalysts with high olefin selectivity and stability by adjusting the types and properties of the support.

3. Silica support

Silica is known for its stable chemical property, weak acidity, large surface area, and rich surface chemistry that can easily disperse the nanoparticles and form strong interactions with active sites by hundreds of silanols. Hence, to eliminate the negative effect of supports, silica may be more suitable for ODH of alkanes.

Lu's group[42] prepared supported boron oxide on high specific area mesoporous silica by incipient wetness impregnation for catalyzing the ODH of propane. The supported boron oxide catalyst (BOS catalyst) exhibited remarkable catalytic properties. The starting active reaction temperature of the BOS catalyst was about 405 °C with a propane conversion of 2.8% and selectivity of 94.6% toward olefins (propylene and ethylene), which is much lower than the h-BN catalyst. When raising the temperature, 73.3% propylene selectivity and 87.4% olefins selectivity (ethylene and propylene) were obtained at 450 °C with a propane conversion of 14.8%. The mesoporous silica support provided an ideal platform to immobilize and transform boron species. The BOS catalyst included the following types of boron species, namely boroxol ring (B(3a)), tri-coordinated hydroxylated linear $BO_{3/2}$ (B(3b)), tri-coordinated planar boron species (B(3c)), and tetra-coordinated boron species fused into the silica framework (B(4)) through ^{11}B NMR characterization (Fig. 2a). The results demonstrated that the tri-coordinated boroxol ring and hydroxylated linear boron species were recognized as active centers for the efficient and low temperature activity of catalytic

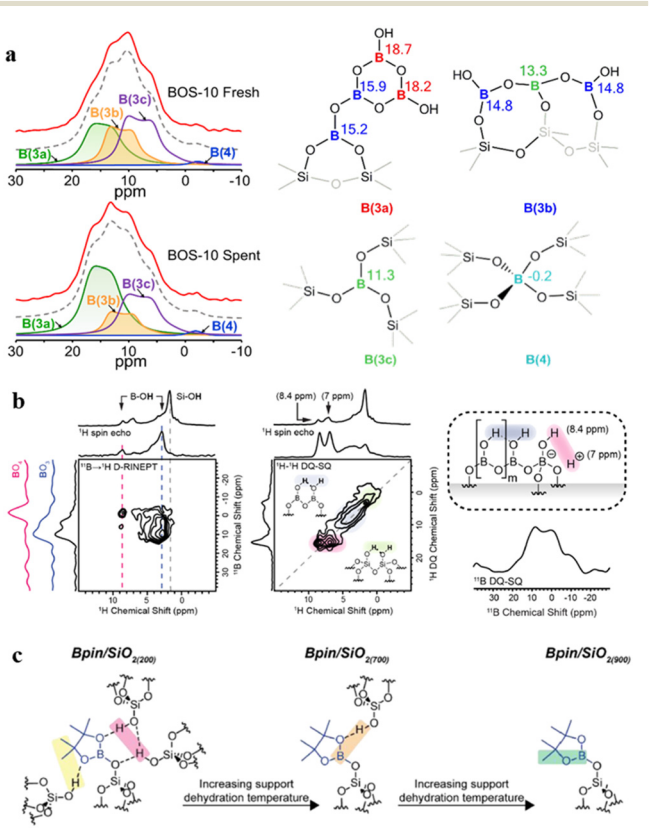

Fig. 2 (a) 1D ^{11}B NMR spectra and boron species of BOS-10 catalysts.[42] Reproduced from ref. 42 with permission from the American Chemical Society, copyright 2019. (b) 2D ^{11}B–^{1}H D-RINEPT NMR, ^{1}H–^{1}H DQ–SQ NMR and 1D DQ–SQ filtered ^{11}B NMR spectra of spent B/SiO_2 catalysts.[43] Reproduced from ref. 43 with permission from the American Chemical Society, copyright 2019. (c) Schematic of $Bpin/SiO_2$ catalyst with Bpin grafted on the surface.[44] Reproduced from ref. 44 with permission from the American Chemical Society, copyright 2021.

ODH of light alkanes. Hermans *et al.*[43] also reported the same catalytic system (B/SiO_2 catalysts) for ODH of propane using triisopropyl borate ($B(O^iPr)_3$) as a boron source. The conversion for the B/SiO_2 catalyst was 5% at 500 °C with 77% propylene selectivity and 91% olefins selectivity. Combined with the NMR, Raman and IR characterizations, the structural information of the boron species was obtained. For example, the 2D ^{11}B–^{1}H D-RINEPT NMR, ^{1}H–^{1}H DQ–SQ NMR and 1D DQ–SQ ^{11}B NMR spectra of spent B/SiO_2 catalysts revealed the presence of BO_3OH and other complex aggregated boron structures (Fig. 2b). The B/SiO_2 catalyst contained agglomerated boron oxide species, consisting of BO_3 unit chains formed by the decomposition of $B(O^iPr)_3$, which may be active for the ODH reaction. Both studies used silica as a support and recognized the structure of active boron species preliminary; it is hard to form different species ranging from isolated to polymeric to nanoparticles for the supported boron oxide system by using the incipient wetness impregnation method, as is usually done with supported metal oxides. Additionally, the leaching of boron on commercial silica under reaction conditions resulted in unstable boron oxide catalysts compared to mesoporous silica.

To further investigate the evolution of active species, the controlled grafting synthesis of pinacolborane on amorphous silica was reported (Bpin/SiO_2(*T*) catalysts).[44] The B–H bond of pinacolborane can react with Si–OH easily, and the steric hindrance of the pinacol ring could inhibit the anchored precursors from being too closely spaced and from undergoing self-reaction. ^{11}B NMR and IR characterizations indicate that the precursor molecule is anchored to the surface monopodally and can interact with adjacent unreacted Si–OH forming hydrogen bonds (Fig. 2c). The amount of neighboring hydrogen-bonded Si–OH species can be adjusted by the silica pretreatment temperature, allowing for a highly controllable local chemical environment around isolated single-anchored Bpin molecules. The boron oxide/hydroxide phase with high mobility can be formed into clusters under thermal treatment on the silica support surface. The species formed on the silica surface can be possibly better controlled by modifications under thermal treatment conditions, chemical treatment of the surface before or after grafting, and doping of the silica surface by decreasing the boron oxide/hydroxide mobility. In addition, Notestein *et al.*[45] used solution-phase deposition to graft boric acids in different sizes on micropores or mesopores of silica supports. For these materials, a high proportion of S2 (hydroxylated non-ring boron) seems to result from a close size matching between the micropores of the silica support and the precursor. The correlation between characterization analysis and the activity of catalysts identified the S2 borate species as the possible active site.

Furthermore, the studies of silica supported boron oxide catalysts deepen the understanding of the mechanism. Wang *et al.*[46] prepared B_2O_3/SiO_2 catalysts by an impregnation method and also identified that the surface tri-coordinated boron sites are the active centers for ODH of propane. The experimental results demonstrated that non-dissociative >B–O–O–B< was formed when O_2 weakly bonds with the electron deficient boron site, reacting directly with propane in the gas phase in ODH of propane. Due to the inhibited adsorption of propylene on >B–O–O–B< sites, high olefins selectivity is achieved over such boron-based catalysts. At the same time, the authors used silica-supported B_2O_3 catalysts in methane conversion to formaldehyde and CO.[47] The O_2 molecules bonded to tri-coordinated BO_3 sites are effective oxidants for methane activation which suppressed the formation of CO_2.

As an efficient support, silica exhibits high olefin selectivity when supporting B_2O_3 compared to metal oxide supports due to its stable chemical property and weak acidity. Besides, the rich surface chemistry such as silanol groups could anchor and affect the boron species. Thus, the synthesis of a supported boron-based catalyst with a more structurally controlled silica could potentially lead to improvement of catalytic properties. To improve the catalytic activity, dendritic fibrous silica (DFNS) was prepared to support BN and B_2O_3.[48] Both DFNS/B_2O_3 and DFNS/BN catalysts displayed higher catalytic activities, and the presence of fibrous morphology and the variety of boron sites attached to silica are responsible for the improved catalytic performance. Kyriakidou *et al.*[49] reported a series of boron-hyperdoped silica catalysts prepared by a laser pyrolysis process which facilitated the establishment of a boron-rich surface. The catalysts produced 6 times higher propylene than commercial boron nitride. Lu *et al.*[50] synthesized porous boron-doped silica fibers by an electrospinning method, which maintained the stability and uniform dispersion of boron species on the silica nanofiber framework. The nanofibers featured one-dimensional and open pore structures that precluded diffusion limitation and ensured high productivity in the ODH reactions. When the conversion of propane was 19.2%, the olefin selectivity and propylene productivities were 90% and 76.6 μmol g_{cat}^{-1} s^{-1}, respectively. The authors also found that the presence of silanol groups may lead to lower olefin selectivity in the ODH reaction.

4. Zeolite

Zeolites are a class of crystalline materials with well-defined porous molecular dimensions, and the large specific surface area, high framework thermal stability, and tunable acidity enable them to be widely used in catalytic processes. Moreover, zeolite materials have proven to be ideal supports for the dispersion and immobilization of active species, including isolated atoms,[51,52] ions,[53,54] clusters[55,56] and nanoparticles.[57] From the catalytic perspective, the characteristics of zeolites greatly influence the reaction process, mainly attributed to the shape-selectivity effects of the microporous structure and coordination environment of active sites. Therefore, it is possible to exploit the unique crystal structure and interaction between active sites and the zeolite framework to develop highly effective boron-based catalysts.

In ODH reactions, the oxygenated boron sites are considered as active species in the ODH reactions over boron-based catalysts. Therefore, embedding boron species into the zeolite matrix can be a promising option for dispersing active sites and thus constructing highly active ODH catalysts. Compared with silica, the diverse crystal structures of zeolites provide more opportunities to modulate the micro-environment of active centers for further tuning the catalytic activity. Therefore, borosilicate zeolites offer the potential to construct highly efficient ODH catalysts. The critical issue is the construction of defective boron sites since boron species are immobilized in the zeolite matrix under different coordination situations, such as trigonally or tetrahedrally coordinated and balanced by different ratios of –OSi and –OH. Previous reports have shown that the tetra-coordinated boron species can be excluded from catalyzing the ODH reaction so that the trigonal boron species are essential in borosilicate zeolites.

For borosilicate zeolite with MWW structure (ERB-1), the isolated $B(OSi)_3$ unit was confirmed inactive for ODH of propane.[58] Meanwhile the aggregated defective trigonal boron site enabled the activation of the C–H bond in propane, confirming that the aggregated BO_3 units were essential in ODH of propane. Moreover, the dynamic transformation of $B(OSi)OH_2$ or $B(OSi)_2OH$ to aggregates suggested that the isolated defect boron sites also contributed to the catalytic activity.[59] Through constructing aggregated boron sites on the B-MWW catalyst, 80.4% propylene selectivity and 91.6% total olefins selectivity (ethylene and propylene) were obtained at 530 °C with a propane conversion of 15.6% (weight-hour-space velocity, WHSV = 4.71 $g_{C_3H_8}\ g_{cat}^{-1}\ h^{-1}$) in ODH of propane. However, the stability of oxygenated boron species in a humid atmosphere is still a challenge due to their hydrolysis-prone nature.

Recently, MFI-type borosilicate zeolite (BS-1) with an isolated boron site of $(–B[OH\cdots O(H)–Si]_2)$ showed durability during the long-period test, maintaining its stable catalytic activity even after washing with water.[60] In combination with 2D $^{11}B \rightarrow {}^{1}H$ HETCOR and time-of-flight mass spectra (ToF-MS), the boron was confirmed to be immobilized in the zeolite framework with a tetra-coordinated (B[4]) structure without any B–O–B species before the ODHP reaction (Fig. 3a). Under ODHP atmosphere, the incomplete hydrolysis of the B[4] site occurred, which resulted in the formation of defect trigonal boron species $(Si–O–B(OH)_2)$. IR and ^{1}H MAS NMR spectra showed the existence of hydrogen bonds between B–OH and its adjacent Si–OH after hydrolysis of B–O–Si (Fig. 3b). By DFT calculation, the existence of hydrogen bonds hindered the deep hydrolysis of boron (energy barrier of 2.05 eV), which maintained the structure of the boron site in the form of $(Si–O–B(OH)_2)$ instead of boric acid $(B(OH)_3)$, guaranteeing the catalytic activity even after washing with water and 200 h durability of ODHP test (Fig. 3c and d). Notably, the hydrogen bonds facilitated the synergistic conversion of oxygen and propane by decreasing the energy barriers, exhibiting an apparent activation energy of 83.7 kJ mol^{-1}, which is almost half that of other boron-based

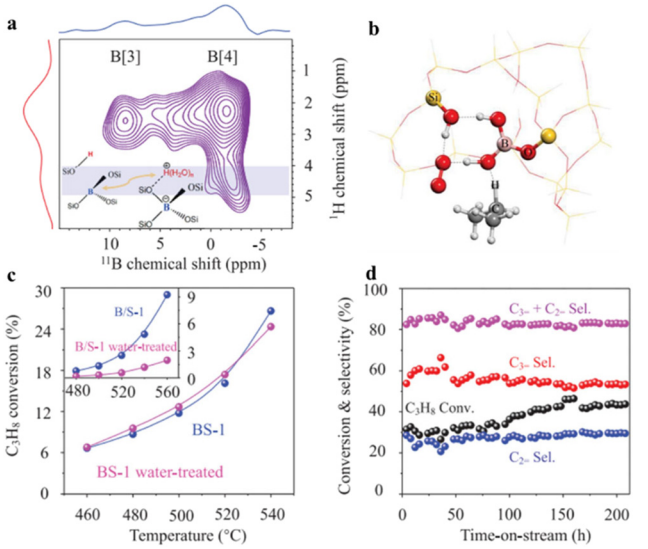

Fig. 3 (a) 2D $^{11}B \rightarrow {}^{1}H$ HETCOR spectra of dehydrated BS-1. (b) Transition state structure of $–B[OH\cdots O(H)–Si]_2$ reacting with propane and oxygen. (c) Data characterizing the BS-1 and B/S-1 catalytic performances before and after water treatment. (d) Data characterizing the stability of BS-1.[60] Reproduced from ref. 60 with permission from the American Association for the Advancement of Science, copyright 2021.

catalysts. A reaction order of 1 for propane was observed, which is significantly distinct from other boron-based catalysts. This catalyst with a B/Si molar ratio of 0.015 showed a propane conversion of 23.8% with propylene and ethylene selectivity of 55.4% and 27.2% at 540 °C (WHSV = 0.71 $g_{C_3H_8}\ g_{cat}^{-1}\ h^{-1}$). Similar results toward active species and kinetic performance were also observed for borosilicate zeolite with *BEA structure, while the MWW structure is still catalytically inactive. In addition, the boron-substituted MCM-41 (B-MCM-41) has recently been reported to exhibit water tolerance.[61] These results suggested that the crystal structure of zeolite might have an important effect when catalyzing the ODHP reaction.

As the silanol groups played a crucial role in immobilizing and modulating active boron centers, enabling the boron species to be anchored in the defect-rich zeolite matrix may be a promising method for constructing highly efficient and stable boron centers. Through decreasing the crystallinity of MFI-type boron-containing zeolite (BMFI-3.0), the catalyst exhibited a propane conversion of 18.0% with an olefin selectivity of 80.4% at 445 °C (WHSV = 37.6 $g_{C_3H_8}\ g_{cat}^{-1}\ h^{-1}$)[62] (Fig. 4a). And a higher olefin productivity of 4.75 $g_{olefin}\ g_{cat}^{-1}\ h^{-1}$ was obtained, compared to previously reported catalysts. ^{11}B, ^{1}H MAS NMR and IR spectra showed that the incomplete crystalline structure facilitated the formation and exposure of defective boron and silica species. Moreover, the ample Si–OH contributed to the formation of hydrogen bonds with B–OH in defective boron species. With the help of *in situ* DRIFT measurements, the isolated boron species were found to transform dynamically into the aggregated state during the ODHP process, and the aggregation process of boron species

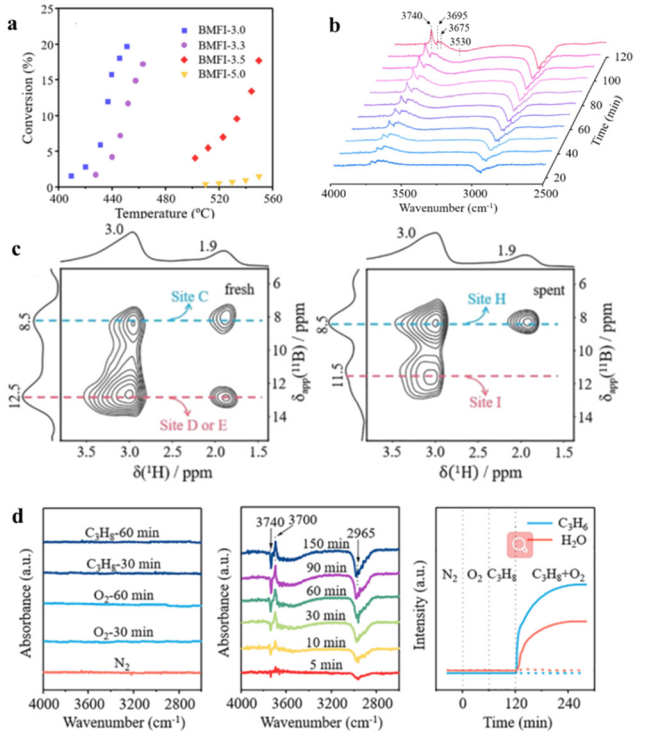

Fig. 4 (a) Effect of temperature on conversion of propane over BMFI catalysts.[62] (b) *In situ* DRIFT difference spectra of fresh BMFI-3.0 catalyst under $C_3H_8/O_2/N_2$ atmosphere at 450 °C.[62] Reproduced from ref. 62 with permission from Elsevier Ltd, copyright 2022. (c) 2D $^{11}B\{^1H\}$ D-HMQC spectra of fresh and spent BZS-3 catalysts.[63] (d) *In situ* DRIFT difference spectra of the fresh BZS-3 catalyst under O_2/N_2, C_3H_8/N_2, and $C_3H_8/O_2/N_2$ atmosphere at 450 °C, and the corresponding mass spectra of C_3H_6 and H_2O species at 450 °C.[63] Reproduced from ref. 63 with permission from the American Chemical Society, copyright 2022.

resulted in the decrease of B–OH groups, which was proved by the decreased intensity of IR bands at 3675 and 3695 cm^{-1} after 50 min of measurement in DRIFT spectra (Fig. 4b). This evolution of boron species is closely matched to the increased reaction rate of propane, indicating that the B–OH groups in aggregated BO_x species that H-bonded to the adjacent silanol groups were responsible for the low temperature catalysis.

Another option is to synthesize two-dimensional nanosheets of zeolite to achieve a higher specific surface area and shorter diffusion paths, thus increasing the amount of accessible silanol groups. Lately, self-pillared boron-containing MFI zeolite nanosheets (BZS-3) with an ultrathin *b*-axis have been reported to catalyze the ODHP reaction at 390 °C.[63] As the temperature was increased to 430 °C, the conversion of propane could reach 14.1%, along with an olefin selectivity of 80.1%. The 2D $^{11}B\{^1H\}$ D-HMQC spectra showed that there were aggregated boron clusters with high mobility (site D and E). After the induction period, site I appeared and showed no correlation with the ^1H NMR signal at *ca.* 1.9 ppm (Fig. 4c). The structure changes of boron species were also monitored by DRIFT, which showed a decrease in the intensity of the Si–OH signal and an increase in B–OH, accompanied by an increase in the propane reaction rate (Fig. 4d). These results suggested that owing to the large specific surface area and enriched silanols, the mobile aggregated boron species could redisperse to oligomeric boron species, revealing a new pathway for the structural evolution of boron species. The redispersion resulted in more active boron centers in the zeolite matrix, which contributed to the enhanced catalytic performance at low temperatures in the ODHP reaction.

5. Boron phosphate

Boron phosphate (BPO_4) is a boron-containing metal-free ternary oxide that can usually act as a ceramic material, petroleum additive, fire retardant, and raw material for synthesizing metal phosphates. BPO_4 usually can be synthesized by mixing H_3PO_4 and H_3BO_3, B_2O_3 and $(NH_4)_2HPO_4$, or B_2O_3 and P_2O_5 then heating in a temperature range from 80 to 1200 °C.[64,65] Besides, some ways of preparing the BPO_4 crystal have also been reported, such as solvothermal synthesis,[66] top-seeding flux growth[67,68] and microwave-assisted method.[65]

BPO_4 is an effective solid acid catalyst with the coexistence of Lewis and Brønsted acidic sites[69] in organic reactions.[70–76] In previous research, BPO_4 also acted as an important selective catalyst for ODH of alkane. Otsuka *et al.*[77–80] reported mixed oxides of boron and phosphorus for partial oxidation of light alkanes, with high light alkane conversion, as well as widespread oxygenated products. Accounting for the mass transfer issues and exposure of active sites during the ODH process, a three-dimensional ordered macroporous boron phosphate material was reported by Lu's group, which had a stable framework and displayed remarkable activity and selectivity during the ODH reaction.[81] The selectivities for propylene and ethylene at 515 °C were 82.5% and 9.0%, respectively, with 14.3% conversion of propane. Meanwhile, the selectivity for the undesired deeply oxidized product carbon dioxide is still less than 1.0%. In addition, the olefin productivity of the BPO_4 catalyst reached as high as ~16 g_{olefin} g_{cat}^{-1} h^{-1}, which is more efficient than most ODH catalysts.

Moreover, BPO_4 with high thermal conductivity, excellent thermal stability, remarkable anisotropic thermal expansion, and prominent oxidation resistance belongs to the group of SiO_2 derivative structures, which may act as a better support.[82–85] A B_2O_3@BPO_4 sandwich-like hollow sphere prepared by a one-step method without templates was used as a liquid phase catalyst for ODH of propane. The B_2O_3@BPO_4 catalyst exhibited excellent propylene productivity (0.79 $g_{C_3H_6}$ g_{cat}^{-1} h^{-1}) at 550 °C and superior stability for 27 h. The loaded B_2O_3 acted as the active species in the molten state, and BPO_4 performed both the role of support and cocatalyst in the ODH reaction.[86] Meanwhile, oxygen vacancy-rich BPO_4 hollow spheres coated by a few layers of h-BN (BN@BPO_4@BN) with a sandwich-like structure were reported to be prepared by an *in situ* high-temperature reduction method.[87] Due to the synergetic effect between

h-BN and oxygen vacancy-rich BPO_4, the prepared catalyst exhibited higher catalytic performance than commercial BN during the ODH of propane. Oxygen vacancy-rich BPO_4 enhanced the adsorption quantity of propane and the confined space at the interface between BN and BPO_4 attenuated the adsorption of propylene, which facilitated the recycling of active sites.

6. Other supports

Activated carbon, which is a kind of carbon-based material with a well-developed internal channel, could be produced from wood, coal, and coconut shell. Due to the resistance of the carbon surface under strongly acidic and basic conditions and the adjustability of the surface chemical properties, this material was often used as a suitable catalyst support.[88] In addition, the average structure of the carbon material consists of aromatic sheets and strips with different gaps between them which were formed during the pyrolysis of the precursor, providing a high surface area and tunable porosity. On the other hand, a variety of defects or functional groups were created on account of the existence of oxygen and hydrogen in the surface group and the unsaturated carbon on the edge of the basal planes.[89] As the support, the goal-oriented modification of carbon was usually involved, including the tailoring of pore distribution and surface chemistry.[90,91]

To stabilize dispersed oxide/hydroxide species and avoid exposure to a hydrophilic surface, Hermans' group[92] reported a carbon-supported boron oxide catalyst prepared by incipient wetness impregnation of boric acid on nitric acid treated activated carbon (B/OAC), exhibiting equal propylene selectivity (propene 87%, olefin 97.4% at 5% propane conversion) and improved productivity compared with h-BN. As mentioned above, the activated carbon that contained –OH and –COOH groups was obtained by nitric acid treatment, which supplied the anchoring sites for boron precursors as well as likely eliminated the combustible carbon site. The SEM–EDX image and C1s XPS (Fig. 5) showed that boron atoms are well-dispersed on the surface of the catalyst and only adventitious carbon is observed. Further analysis indicated that slight boron leaching occurred during the reaction, which could be ascribed to the hydrophobicity of the catalyst. It was revealed by the 2D ^{11}B MQMAS solid-state NMR spectra of the fresh and spent catalysts that the B/OAC catalyst contained five unique boron species: $B(OB)_x(OH)_{3-x}$ (x = 1–2), $B(OB)_3$, $B(OB)_2(OC)$, $B(OB)(OC)_2$, and $B(OC)_3$. The consumption of C═O/C–O during the preparation process confirmed by DRIFTS suggested that the $B(OB)_2(OC)$, $B(OB)(OC)_2$ boron atoms might be anchored by surface functional groups. To understand the distribution of the boron phase, *in situ* Raman spectroscopic investigation was conducted, which demonstrated the minimal differences between fresh and spent B/OAC, suggesting that the boron structure might change dynamically during the reaction, while the materials recovered once removing the reaction condition.

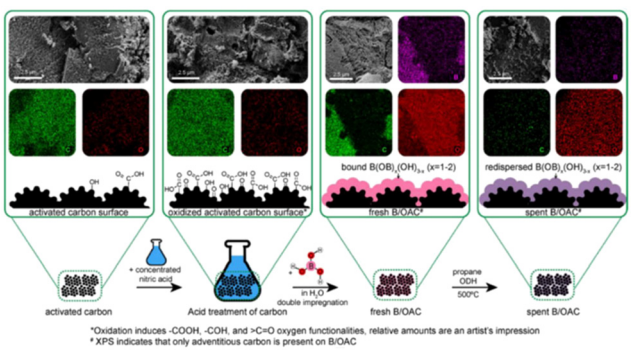

Fig. 5 Schematic and SEM/EDX images of the synthesis for B/OAC catalyst.[92] Reproduced from ref. 92 with permission from John Wiley and Sons, copyright 2021.

Removing heat is important for practical application because the strong exothermicity of the ODH reaction could lead to hotspots and thus cause a negative impact on the selectivity to olefins or even safety. Typically, there are two methods to suppress the influence of hotspots: using a high thermal conductivity catalyst material and increasing the space velocity. Cordierite monolith, which is widely used in the area of environmental catalysis, is characterized by its inferior thermal expansivity, superior stability, and excellent mechanical strength.[93] To achieve a high catalytic activity at high space velocity, a silica and boron oxide sequentially coated cordierite catalyst (B_2O_3/SiO_2@HC) was prepared through a two-step wash-coat method. The catalyst was used for the ODHP reaction with a remarkable performance (86.0% $C_3^=$ and 11.6% $C_2^=$ at propane conversion of 16.9%) under a high gas hourly space velocity (GHSV) of 345 600 ml $g_{B_2O_3}^{-1}$ h^{-1} (Fig. 6a).[94] Furthermore, h-BN wash-coated cordierite monolithic (h-BN/cordierite) was prepared by CVD and exhibited 82.1% selectivity to propylene and 3.7% selectivity to CO with no detectable CO_2 at 16.8% propane conversion with a high GHSV of 576 000 ml g_{BN}^{-1} h^{-1} (Fig. 6b).[95] The *in situ* synthesis of h-BN on cordierite avoided the internal diffusion resistance which is caused by the conventional secondary support and ensured the mass transfer at high GHSV with a propylene productivity of 18.6 $g_{C_3H_6}$ g_{BN}^{-1}.

Characterized with chemically inert nature, h-BN was often employed as a support of catalysis in catalytic reaction systems, such as selective oxidation,[8] ammonia synthesis,[96,97] CO oxidation,[98] and Fischer–Tropsch synthesis.[99] In the ODH reaction of ethylbenzene, BN-supported monomeric MoO_x catalysts were designed for the selective coproduction of styrene and benzaldehyde.[100] *In situ* FTIR analysis was further carried out to verify the role of hydroxy groups in the reaction process, suggesting that these boron hydroxyl groups might guide the reaction pathways by assisting the monomeric MoO_x species and favorably forming the product, benzaldehyde. Beyond the MoO_x species, the boron nitride-supported FeO_x catalyst was also reported, in which the selectivity to styrene was up to 94% at 60% ethylbenzene conversion under oxygen-rich conditions.[101] Based on the reaction kinetics and a series of characterizations, the BO_x

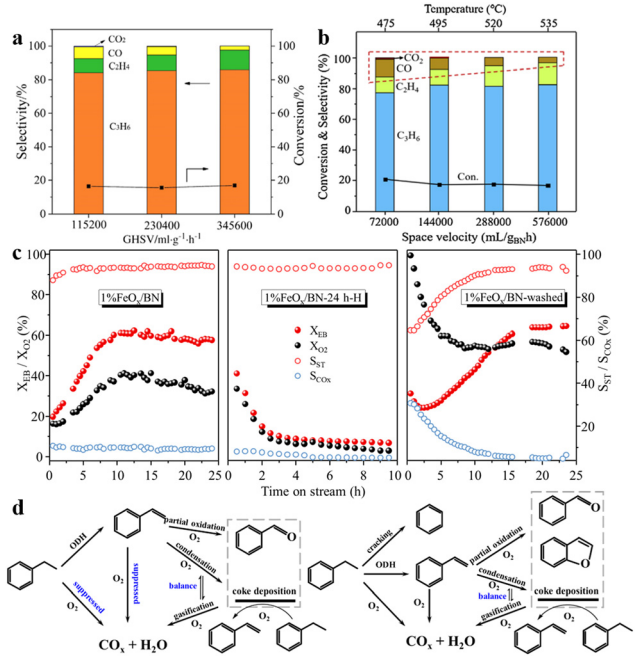

Fig. 6 (a) Influence of GHSV on the conversion of propane and selectivity to products over B_2O_3/SiO_2@HC catalyst.[94] Reproduced from ref. 94 with permission from Elsevier Ltd, copyright 2020. (b) Influence of temperatures and space velocities on the conversion of propane and selectivity to products over the h-BN/cordierite catalyst.[95] Reproduced from ref. 95 with permission from Elsevier Ltd, copyright 2020. (c) Catalytic performance for ODH of EB over supported FeO_x catalysts.[101] (d) Possible reaction pathways of 1% FeO_x/BN and 1% FeO_x/SBA-15 catalysts for the ODH of EB.[101] Reproduced from ref. 101 with permission from Elsevier Ltd, copyright 2022.

derived from the BN support was considered to strongly interact with the FeO_x cluster, hindering the over-oxidation of ethylbenzene. To elucidate the role of the activated components and BN support, the HCl-washed catalyst and the water-washed catalyst were considered (Fig. 6c). The washed 1% FeO_x/BN had a higher initial EB conversion (30%) with an obvious induction period while the selectivity was close to that of other catalysts, such as 1% FeO_x/SBA-15, 1% FeO_x/SiC, and bulk Fe_2O_3 samples, indicating the re-formation of BO_x species and the interaction between the FeO_x species and BN support. Combined with the analysis of the reaction pathways (Fig. 6d), one could conclude that: the dehydrogenation was firstly initiated by the redox FeO_x species and then newly formed coke deposition with quinone/carbonyl sites on the FeO_x/BN catalyst led to the promoted activity in the induction period. The balance of coke deposition and its gasification rates was finally achieved with the aid of the FeO_x and BO_x species under oxygen-rich conditions. In addition to FeO_x and MoO_x, Wu *et al.*[102] reported that VO_x onto h-BN (VO_x/BN-*T*), in which the vanadium oxide facilitates the oxyfunctionalization of BN by concurrently producing nitric oxide to trigger additional gas-phase radical. Moreover, VO_x sites catalyzed the reaction through the redox cycles. In view of the studies of h-BN supported metallic oxide catalysts as mentioned above, the strong metal–support interaction (SMSI) concept was further broadened owing to the unique nature of BO_x species derived from the h-BN support.

7. Summary and outlook

Boron-based catalysts have opened up a new route for the conversion of light alkanes to their corresponding alkenes with the feature of superior anti-oxidation ability compared with metal-based catalysts. The supported boron-based catalysts with high dispersion of active sites and tunable properties of supports show great potential in understanding the reaction mechanism and developing highly active and selective boron-based catalysts. More efforts are needed to be devoted to revealing the unique characteristics of supports and their influence in catalyzing ODH reactions of light alkanes. The catalytic performance of supported catalysts in ODH systems is shown in Table 1. Metal oxide supported boron-based catalysts generally have lower olefin selectivity and produce more CO_x. The metal oxide supports could disperse boron species, while their strong acidity and non-stoichiometric oxygen on the surface often resulted in a significant amount of deep-oxidation products and oxygenates, leading to decreased olefin selectivity. Moreover, the loss of active boron sites was also a serious problem due to the weak interaction with the metal oxide. Therefore, the metal oxide may not be the ideal support for constructing boron-based catalysts. Silica supports show no strong acidic or alkaline properties, and their large surface area and surface defect sites provide a suitable environment for dispersing and stabilizing boron species. These properties allow the ample exposure of active boron species as well as stability during the ODH reaction. Consequently, silica-supported boron-based catalysts are capable of inhibiting deep oxidation of propylene and catalyzing ODH reactions at much lower reaction temperatures. Boron-containing zeolite materials are made of a crystalline silica framework and uniform distribution of boron atoms. Compared with amorphous silica supports, except for the anchoring effect of silanols, their interaction with adjacent boron atoms enables the modification of the electronic environment of oxygenated boron species, which contributes to a lower reaction energy barrier for the ODH reaction. It is worth noting that another function of the silanol group is to inhibit the leaching of the framework boron atoms, which provides insight into the preparation of stable boron-based catalysts. When boron phosphate was used as a support, there was a smaller amount of deep-oxidation product CO_x, which may be due to the enhanced electron density of tetra-coordinated boron species in the boron phosphate and inhibited the breaking of C–C bonds. Notably, the support with high thermal conductivity and better mass transfer is helpful to improve the productivity of olefins, such as B_2O_3/SiO_2@HC and h-BN/cordierite catalysts.

For supported boron-based catalysts, the structure of active boron species is usually studied by ^{11}B NMR, Raman and IR characterization. We summarize the general structure of boron species for the supported boron-based catalysts

Table 1 Catalytic performance of supported boron-based catalysts in ODH systems

Supports	Catalysts	Temp (°C)	Con. (%)	Selectivity (%)				Productivity ($g_{olefin}\ g_{cat}^{-1}\ h^{-1}$)	Ref.
				$C_3^=$	$C_2^=$	CO	CO_2		
Metal oxide	C_2H_6								
	B_2O_3–Al_2O_3	550	38.0		58.0	31.0	1.6	0.33	33
	B_2O_3–La_2O_3	550	5.7		82.6	8.2	1.3	0.07	33
	B_2O_3–MgO	550	4.6		80.0	8.5	2.8	0.05	33
	B_2O_3–TiO_2	550	0.4		98.0	—	—	0.01	33
	B_2O_3–CaO	550	5.8		30.2	30.3	39.0	0.03	33
	B_2O_3–ZnO	550	35.0		40.6	2.7	56.5	0.21	33
	Alumina–boria	550	18.7		89.3	9.1	—	0.63	35
	C_3H_8								
	B_2O_3(0.17 wt%)/γ-Al_2O_3	550	24.8	18.8	3.4	44.0	33.9	0.02	38
	B_2O_3/Al_2O_3(A)	550	42.0	40.0	23.0	19.0	5.0	0.63	40
	B_2O_3/Al_2O_3(B)	550	30.0	42.0	13.0	11.0	2.0	0.21	40
	B_2O_3/Al_2O_3(C)	550	4.0	46.0	5.0	28.0	17.0	0.03	40
	B_2O_3/Al_2O_3(D)	550	28.0	41.0	12.0	27.0	14.0	0.37	40
	B_2O_3/MgO	550	20.0	27.0	12.0	21.0	35.0	0.19	40
	B_2O_3/TiO_2	550	8.0	74.0	11.0	4.0	1.0	0.18	40
	B_2O_3/ZrO_2	550	15.0	68.0	14.0	5.0	<1	0.31	40
Silica	BOS-10	450	14.8	73.3	14.1	10.8	1.8	1.1	42
	B/SiO_2	500	5.0	76.9	14	5.5	1.6	—	43
	Bpin/SiO_2(*T*)	500	5.0	75.0	—	—	—	—	44
	P5-c	500	6.0	82.0	8.0	5.0	2.0	0.05	45
	32.8%B_2O_3/SiO_2	550	10.0	76.0	18.0	2.0	1.0	0.3	46
	DFNS/B_2O_3	490	24.7	22.5	7.5	54.0	14.0	1.0	48
	DFNS/BN	490	25.5	57.0	15.0	14.0	5.0	1.9	48
	25 at% boron-hyper doped silicon	450	10.6	64.1	7.2	9.7	2.5	1.97	49
	PBSN	545	19.2	74.5	14.4	9.8		13.07	50
Zeolite	B-MWW	540	29.9	72.5	15.3	11.3	0.9	1.11	59
	BS-1	540	23.8	55.4	27.2	—	—	0.12	60
	B-MCM-41	550	14.5	48.7	31.0	3.8	12.0	0.40	61
	BMFI-3.0	445	18.0	60.3	20.1	18.5	1.1	4.75	62
	BZS-3	430	14.1	60.1	20.0	19.9		0.93	63
Boron phosphate	B_2O_3@BPO_4	550	24.7	66.4	18.4	5.2	0.2	0.87	86
	BN@BPO_4@BN	550	13.6	75.2	—	—	—	0.03	87
Other	B/OAC	500	5.0	87.0	8.4	2.3	0.45	—	92
	B_2O_3/SiO_2@HC	535	16.9	86.0	11.6	2.3	0.1	17.1[a]	94
	h-BN/cordierite	535	16.8	82.1	14.2	3.7	—	20.7[a]	95
	VO_x/BN-*T*	600	68.7	—	—	—	—	—	102

[a] The units of productivity for h-BN/cordierite and B_2O_3/SiO_2@HC are $g_{olefin}\ g_{BN}^{-1}\ h^{-1}$ and $g_{olefin}\ g_{B_2O_3}^{-1}\ h^{-1}$, respectively.

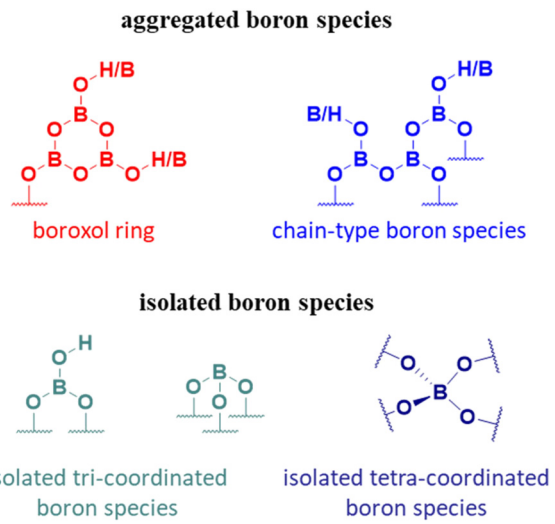

Fig. 7 Structure schematic of boron species for supported boron-based catalysts.

(Fig. 7). The isolated boron species are usually formed by the interaction of boron precursors with the hydroxyl groups on the support and anchored to the framework. These species are stable and less likely to be leached, but are poorly reactive in the ODH reaction. The aggregated boron species are more likely to form on the support surface due to the high mobility of oxidized boron and the thermodynamic stability of boroxol-rich models. These species also can be formed dynamically during the ODH reaction and are highly active species. Besides, the types of boron species are affected by different precursors, defects on the support surface, boron content, and treatment methods.

Although a wealth of effort has demonstrated the promising potential of supported boron-based catalysts, there are still some challenges that need to be further addressed. The first is the identification of the structure of the active boron species under reaction conditions. The aggregated boron clusters are considered to be more active, but the structural evolution under ODH conditions leads to

difficulties in the identification of their precise structure. It is urgent to develop *in situ* and high-time resolution characterization to describe the geometric and electronic structures of active boron species during the dynamic evolution in the ODH reaction. The second is the improvement of olefin selectivity in ODH reactions. For silica supports, in addition to the positive influence of silanol groups, the existence of silanol groups may influence the reaction pathway, which results in a lower propylene selectivity compared with BN materials. The most important issue is the catalytic stability of boron sites under ODH conditions, as the boron atom readily hydrolyzes with water and detaches from the catalytic system. Hence, in order to develop highly active and selective supported boron-based catalysts, targeted construction of highly active boron species is essential. Furthermore, the utilization of supports to modify the local microenvironment of active boron centers modulates the reaction path to improve the catalytic activity and selectivity. For silica materials, the construction of defective sites, such as Si–OH, ≡Si–O$^{\bullet}$, or ≡Si$^{\bullet}$, may be a feasible way to modulate the electronic structure of the active boron centers, alter the reaction pathways, and thus develop highly active and selective catalysts. The stabilization of boron species may be possible through nanostructure engineering that localizes them in a confined space while enhancing interactions with the supports. Overall, high efficiency supported boron-based catalysts can be rationally designed, and the multiple impacts from boron species and supports characteristics should be carefully assessed for fruitful catalysis.

Conflicts of interest

There are no conflicts to declare.

Acknowledgements

This work was supported by the State Key Program of the National Natural Science Foundation of China (21733002), the National Natural Science Foundation of China (22108028), the National Key Research and Development Program of China (2018YFA0209404), and the Program for Liaoning Innovative Research Team in University (LT2016001).

Notes and references

1 J. J. Sattler, J. Ruiz-Martinez, E. Santillan-Jimenez and B. M. Weckhuysen, *Chem. Rev.*, 2014, **114**, 10613–10653.
2 A. Corma, F. V. Melo, L. Sauvanaud and F. Ortega, *Catal. Today*, 2005, **107–108**, 699–706.
3 Y. Gao, L. Neal, D. Ding, W. Wu, C. Baroi, A. M. Gaffney and F. Li, *ACS Catal.*, 2019, **9**, 8592–8621.
4 F. Cavani, N. Ballarini and A. Cericola, *Catal. Today*, 2007, **127**, 113–131.
5 S. Najari, S. Saeidi, P. Concepcion, D. D. Dionysiou, S. K. Bhargava, A. F. Lee and K. Wilson, *Chem. Soc. Rev.*, 2021, **50**, 4564–4605.
6 E. McFarland, *Science*, 2012, **338**, 340–342.
7 J. T. Grant, J. M. Venegas, W. P. McDermott and I. Hermans, *Chem. Rev.*, 2018, **118**, 2769–2815.
8 L. Shi, Y. Wang, B. Yan, W. Song, D. Shao and A. H. Lu, *Chem. Commun.*, 2018, **54**, 10936–10946.
9 J. H. Carter, T. Bere, J. R. Pitchers, D. G. Hewes, B. D. Vandegehuchte, C. J. Kiely, S. H. Taylor and G. J. Hutchings, *Green Chem.*, 2021, **23**, 9747–9799.
10 W. P. McDermott, M. C. Cendejas and I. Hermans, *Top. Catal.*, 2020, **63**, 1700–1707.
11 S. R. G. Carrazán, C. Peres, J. P. Bernard, M. Ruwet, R. Ruiz and B. Delmon, *J. Catal.*, 1996, **158**, 452–476.
12 M. A. De León, C. De Los Santos, L. Latrónica, A. M. Cesio, C. Volzone, J. Castiglioni and M. Sergio, *Chem. Eng. J.*, 2014, **241**, 336–343.
13 Y.-M. Liu, Y. Cao, N. Yi, W.-L. Feng, W.-L. Dai, S.-R. Yan, H.-Y. He and K.-N. Fan, *J. Catal.*, 2004, **224**, 417–428.
14 C. A. Gärtner, A. C. van Veen and J. A. Lercher, *ChemCatChem*, 2013, **5**, 3196–3217.
15 W. H. K. Ng, E. S. Gnanakumar, E. Batyrev, S. K. Sharma, P. K. Pujari, H. F. Greer, W. Zhou, R. Sakidja, G. Rothenberg, M. W. Barsoum and N. R. Shiju, *Angew. Chem., Int. Ed.*, 2018, **57**, 1485–1490.
16 T. Wang, X. Guan, H. Lu, Z. Liu and M. Ji, *Appl. Surf. Sci.*, 2017, **398**, 1–8.
17 Z. Li, A. W. Peters, A. E. Platero-Prats, J. Liu, C. W. Kung, H. Noh, M. R. DeStefano, N. M. Schweitzer, K. W. Chapman, J. T. Hupp and O. K. Farha, *J. Am. Chem. Soc.*, 2017, **139**, 15251–15258.
18 J. Sheng, B. Yan, W. D. Lu, B. Qiu, X. Q. Gao, D. Wang and A. H. Lu, *Chem. Soc. Rev.*, 2021, **50**, 1438–1468.
19 C. A. Carrero, R. Schloegl, I. E. Wachs and R. Schomaecker, *ACS Catal.*, 2014, **4**, 3357–3380.
20 J. T. Grant, C. A. Carrero, F. Goeltl, J. Venegas, P. Mueller, S. P. Burt, S. E. Specht, W. P. McDermott, A. Chieregato and I. Hermans, *Science*, 2016, **354**, 1570–1573.
21 L. Shi, D. Wang, W. Song, D. Shao, W.-P. Zhang and A.-H. Lu, *ChemCatChem*, 2017, **9**, 1788–1793.
22 R. Huang, B. Zhang, J. Wang, K.-H. Wu, W. Shi, Y. Zhang, Y. Liu, A. Zheng, R. Schlögl and D. S. Su, *ChemCatChem*, 2017, **9**, 3293–3297.
23 L. Shi, B. Yan, D. Shao, F. Jiang, D. Wang and A.-H. Lu, *Chin. J. Catal.*, 2017, **38**, 389–395.
24 J. M. Venegas, J. T. Grant, W. P. McDermott, S. P. Burt, J. Micka, C. A. Carrero and I. Hermans, *ChemCatChem*, 2017, **9**, 2118–2127.
25 J. T. Grant, W. P. McDermott, J. M. Venegas, S. P. Burt, J. Micka, S. P. Phivilay, C. A. Carrero and I. Hermans, *ChemCatChem*, 2017, **9**, 3623–3626.
26 L. Shi, D. Wang and A.-H. Lu, *Chin. J. Catal.*, 2018, **39**, 908–913.
27 B. Yan, W.-C. Li and A.-H. Lu, *J. Catal.*, 2019, **369**, 296–301.
28 J. M. Venegas and I. Hermans, *Org. Process Res. Dev.*, 2018, **22**, 1644–1652.
29 S. Soled, *Science*, 2015, **350**, 1171–1172.

30 Q. Chen, Y. Nie, M. Ming, G. Fan, Y. Zhang and J.-S. Hu, *Chin. J. Catal.*, 2020, **41**, 1791–1811.
31 F. Rebillat, in *Advances in Ceramic Matrix Composites*, 2014, pp. 369–409.
32 K. Otsuka and M. Hatano, *J. Catal.*, 1987, **108**, 252–255.
33 Y. Murakami, K. Otsuka, Y. Wada and A. Morikawa, *Chem. Lett.*, 1989, 535–538.
34 Y. Murakami, K. Otsuka, Y. Wada and A. Morikawa, *Bull. Chem. Soc. Jpn.*, 1990, **63**, 340–346.
35 G. Colorio, J. C. Vedrine, A. Auroux and B. Bonnetot, *Appl. Catal., A*, 1996, **137**, 55–68.
36 K. Otsuka, T. Ando, S. Suprapto, Y. Wang, K. Ebitani and I. Yamanaka, *Catal. Today*, 1995, **24**, 315–320.
37 T. Komatsu, Y. Uragami and K. Otsuka, *Chem. Lett.*, 1988, 1903–1906.
38 O. V. Buyevskaya, M. Kubik and M. Baerns, in *Heterogeneous Hydrocarbon Oxidation*, ed. B. K. Warren and S. T. Oyama, 1996, vol. 11, pp. 155–169.
39 O. V. Buyevskaya and M. Baerns, *Catal. Today*, 1998, **42**, 315–323.
40 O. V. Buyevskaya, D. Müller, I. Pitsch and M. Baerns, *Stud. Surf. Sci. Catal.*, 1998, **119**, 671–676.
41 L. Leveles, *J. Catal.*, 2003, **218**, 296–306.
42 W.-D. Lu, D. Wang, Z. Zhao, W. Song, W.-C. Li and A.-H. Lu, *ACS Catal.*, 2019, **9**, 8263–8270.
43 A. M. Love, M. C. Cendejas, B. Thomas, W. P. McDermott, P. Uchupalanun, C. Kruszynski, S. P. Burt, T. Agbi, A. J. Rossini and I. Hermans, *J. Phys. Chem. C*, 2019, **123**, 27000–27011.
44 M. C. Cendejas, R. W. Dorn, W. P. McDermott, E. A. Lebrón-Rodríguez, L. O. Mark, A. J. Rossini and I. Hermans, *J. Phys. Chem. C*, 2021, **125**, 12636–12649.
45 H. Yan, S. Alayoglu, W. Wu, Y. Zhang, E. Weitz, P. C. Stair and J. M. Notestein, *ACS Catal.*, 2021, 9370–9376.
46 J. Tian, J. Li, S. Qian, Z. Zhang, S. Wan, S. Wang, J. Lin and Y. Wang, *Appl. Catal., A*, 2021, **623**, 118271.
47 J. Tian, J. Tan, Z. Zhang, P. Han, M. Yin, S. Wan, J. Lin, S. Wang and Y. Wang, *Nat. Commun.*, 2020, **11**, 5693.
48 R. Belgamwar, A. G. M. Rankin, A. Maity, A. K. Mishra, J. S. Gómez, J. Trébosc, C. P. Vinod, O. Lafon and V. Polshettiwar, *ACS Sustainable Chem. Eng.*, 2020, **8**, 16124–16135.
49 J. Chen, P. Rohani, S. G. Karakalos, M. J. Lance, T. J. Toops, M. T. Swihart and E. A. Kyriakidou, *Chem. Commun.*, 2020, **56**, 9882–9885.
50 B. Yan, W.-D. Lu, J. Sheng, W.-C. Li, D. Ding and A.-H. Lu, *Chin. J. Catal.*, 2021, **42**, 1782–1789.
51 Y. Zhang, L. Qi, A. Lund, P. Lu and A. T. Bell, *J. Am. Chem. Soc.*, 2021, **143**, 8352–8366.
52 L. Qi, Y. Zhang, M. A. Conrad, C. K. Russell, J. Miller and A. T. Bell, *J. Am. Chem. Soc.*, 2020, **142**, 14674–14687.
53 X. Deng, R. Bai, Y. Chai, Z. Hu, N. Guan and L. Li, *CCS Chem.*, 2022, **4**, 949–962.
54 Z. Maeno, S. Yasumura, X. Wu, M. Huang, C. Liu, T. Toyao and K. I. Shimizu, *J. Am. Chem. Soc.*, 2020, **142**, 4820–4832.
55 J. Zhu, R. Osuga, R. Ishikawa, N. Shibata, Y. Ikuhara, J. N. Kondo, M. Ogura, J. Yu, T. Wakihara, Z. Liu and T. Okubo, *Angew. Chem., Int. Ed.*, 2020, **59**, 19669–19674.
56 Q. Sun, N. Wang, Q. Fan, L. Zeng, A. Mayoral, S. Miao, R. Yang, Z. Jiang, W. Zhou, J. Zhang, T. Zhang, J. Xu, P. Zhang, J. Cheng, D. C. Yang, R. Jia, L. Li, Q. Zhang, Y. Wang, O. Terasaki and J. Yu, *Angew. Chem., Int. Ed.*, 2020, **59**, 19450–19459.
57 Y. Wang, C. Wang, L. Wang, L. Wang and F. S. Xiao, *Acc. Chem. Res.*, 2021, **54**, 2579–2590.
58 N. Altvater, R. Dorn, M. Cendejas, W. McDermott, B. Thomas, A. Rossini and I. Hermans, *Angew. Chem., Int. Ed.*, 2020, **59**, 6546–6550.
59 B. Qiu, F. Jiang, W.-D. Lu, B. Yan, W.-C. Li, Z.-C. Zhao and A.-H. Lu, *J. Catal.*, 2020, **385**, 176–182.
60 H. Zhou, X. Yi, Y. Hui, L. Wang, W. Chen, Y. Qin, M. Wang, J. Ma, X. Chu, Y. Wang, X. Hong, Z. Chen, X. Meng, H. Wang, Q. Zhu, L. Song, A. Zheng and F.-S. Xiao, *Science*, 2021, **372**, 76–80.
61 Q. Liu, J. Wang, Z. Liu, R. Zhao, A. Xu and M. Jia, *ACS Omega*, 2022, **7**, 3083–3092.
62 B. Qiu, W.-D. Lu, X.-Q. Gao, J. Sheng, B. Yan, M. Ji and A.-H. Lu, *J. Catal.*, 2022, **408**, 133–141.
63 B. Gao, B. Qiu, M. Zheng, Z. Liu, W.-D. Lu, Q. Wang, J. Xu, F. Deng and A.-H. Lu, *ACS Catal.*, 2022, **12**, 7368–7376.
64 M. Abat, F. Degryse, R. Baird and M. J. McLaughlin, *J. Plant Nutr. Soil Sci.*, 2014, **177**, 860–868.
65 A. Baykal, M. Kizilyalli, M. Toprak and R. Kniep, *Turk. J. Chem.*, 2001, **25**, 425–432.
66 M. Schmidt, B. Ewald, Y. Prots, R. Cardoso-Gil, M. Armbrüster, I. Loa, L. Zhang, Y.-X. Huang, U. Schwarz and R. Kniep, *Z. Anorg. Allg. Chem.*, 2004, **630**, 655–662.
67 Z. Li, Y. Wu, P. Fu, S. Pan and C. Chen, *J. Cryst. Growth*, 2004, **270**, 486–490.
68 Z. Li, Z. Lin, Y. Wu, P. Fu, Z. Wang and C. Chen, *Chem. Mater.*, 2004, **16**, 2906–2908.
69 Z. Xue, X. Zhao, J. Wang and T. Mu, *Chem. – Asian J.*, 2017, **12**, 2271–2277.
70 O. A. Rusu, W. F. Hoelderich, H. Wyart and M. Ibert, *Appl. Catal., B*, 2015, **176–177**, 139–149.
71 J. B. Moffat and S. S. Jewur, *J. Catal.*, 1982, **75**, 94–100.
72 A. Tada, H. Suzuka and Y. Imizu, *Chem. Lett.*, 1987, **16**, 423–424.
73 S. Imamura, K. Imakubo, S. Furuyoshi and H. Jindai, *Ind. Eng. Chem. Res.*, 1991, **30**, 2355–2358.
74 H. L. Goltz and J. B. Moffat, *J. Catal.*, 1971, **22**, 85–95.
75 H. Tsuji and T. Setoyama, *Chem. Lett.*, 2005, **34**, 1232–1233.
76 J. Morey, J. M. Marinas and J. V. Sinisterra, *React. Kinet. Catal. Lett.*, 1983, **22**, 175–180.
77 K. Otsuka, Y. Uragami, T. Komatsu and M. Hatano, *Stud. Surf. Sci. Catal.*, 1991, **61**, 15–23.
78 T. Komatsu, Y. Uragami and K. Otsuka, *Chem. Lett.*, 1988, **17**, 1903–1906.
79 Y. Uragami and K. Otsuka, *J. Chem. Soc., Faraday Trans.*, 1992, **88**, 3605–3610.

80 K. Otsuka, Y. Uragami and M. Hatano, *Catal. Today*, 1992, **13**, 667–672.
81 W.-D. Lu, X.-Q. Gao, Q.-G. Wang, W.-C. Li, Z.-C. Zhao, D.-Q. Wang and A.-H. Lu, *Chin. J. Catal.*, 2020, **41**, 1837–1845.
82 A. Adamczyk and M. Handke, *J. Mol. Struct.*, 2000, **555**, 159–164.
83 F. A. Hummel and T. A. Kupinski, *J. Am. Chem. Soc.*, 1950, **72**, 5318–5319.
84 S. N. Achary and A. K. Tyagi, *J. Solid State Chem.*, 2004, **177**, 3918–3926.
85 S. Zhao, G. Zhang, K. Feng, J. Lu and Y. Wu, *Cryst. Res. Technol.*, 2012, **47**, 391–396.
86 Q. Liu, Y. Wu, F. Xing, Q. Liu, X. Guo and C. Huang, *J. Catal.*, 2020, **381**, 599–607.
87 Q. Liu, C. Chen, Q. Liu, Y. Wu, F. Xing, C. Cheng and C. Huang, *Appl. Surf. Sci.*, 2021, **537**, 147927.
88 M. Iwanow, T. Gartner, V. Sieber and B. Konig, *Beilstein J. Org. Chem.*, 2020, **16**, 1188–1202.
89 F. Rodríguez-Reinoso, *Carbon*, 1998, **36**, 159–175.
90 S. B. Lyubchik, R. Benoit and F. Béguin, *Carbon*, 2002, **40**, 1287–1294.
91 A. Bhatnagar, W. Hogland, M. Marques and M. Sillanpää, *Chem. Eng. J.*, 2013, **219**, 499–511.
92 L. O. Mark, R. W. Dorn, W. P. McDermott, T. O. Agbi, N. R. Altvater, J. Jansen, E. A. Lebrón-Rodríguez, M. C. Cendejas, A. J. Rossini and I. Hermans, *ChemCatChem*, 2021, **13**, 3611–3618.
93 W. M. Carty and P. W. Lednor, *Curr. Opin. Solid State Mater. Sci.*, 1996, **1**, 88–95.
94 Y. Zhou, Y. Wang, W. Lu, B. Yan and A. Lu, *Chin. J. Chem. Eng.*, 2020, **28**, 2778–2784.
95 Y. Wang, W.-C. Li, Y.-X. Zhou, R. Lu and A.-H. Lu, *Catal. Today*, 2020, **339**, 62–66.
96 C. J. H. Jacobsen, *J. Catal.*, 2001, **200**, 1–3.
97 T. W. Hansen, J. B. Wagner, P. L. Hansen, S. Dahl, H. Topsøe and C. J. H. Jacobsen, *Science*, 2001, **294**, 1508–1510.
98 T.-M. Tran-Thuy, C.-C. Chen and S. D. Lin, *ACS Catal.*, 2017, **7**, 4304–4312.
99 J. Wu, L. Wang, X. Yang, B. Lv and J. Chen, *Ind. Eng. Chem. Res.*, 2018, **57**, 2805–2810.
100 J. Sheng, W.-C. Li, Y.-R. Wang, W.-D. Lu, B. Yan, B. Qiu, X.-Q. Gao, S.-Q. Cheng, L. He and A.-H. Lu, *J. Catal.*, 2021, **400**, 265–273.
101 J. Sheng, W.-C. Li, W.-D. Lu, B. Yan, B. Qiu, X.-Q. Gao, R.-P. Zhang, S.-Z. Zhou and A.-H. Lu, *Appl. Catal., B*, 2022, **305**, 121070.
102 X. Jiang, X. Zhang, S. C. Purdy, Y. He, Z. Huang, R. You, Z. Wei, H. M. Meyer, J. Yang, Y. Pan, P. Wu, W. Zhu, M. Chi, K. Page, W. Huang and Z. Wu, *JACS Au*, 2022, **2**, 1096–1104.